UNIVERSITY OF BIRMINGHAM
University of Birmingham Research at Birmingham

Topotactic fluorine insertion into the channels of FeSb2O4-related materials.

Greaves, Colin; de Laune, Benjamin; Rees, Gregory; Marco, Jose; Hah, Hien-Yoong; Johnson, Charles; Johnson, Jacqueline; Berry, Frank; hanna, john

DOI:
10.1021/acs.inorgchem.7b01613

License:
Creative Commons: Attribution (CC BY)

Document Version
Publisher's PDF, also known as Version of record

Citation for published version (Harvard):
Greaves, C, de Laune, B, Rees, G, Marco, J, Hah, H-Y, Johnson, C, Johnson, J, Berry, F & hanna, J 2017, 'Topotactic fluorine insertion into the channels of FeSb2O4-related materials.', *Inorganic Chemistry*, pp. 10078–10089. https://doi.org/10.1021/acs.inorgchem.7b01613

Link to publication on Research at Birmingham portal

General rights
Unless a licence is specified above, all rights (including copyright and moral rights) in this document are retained by the authors and/or the copyright holders. The express permission of the copyright holder must be obtained for any use of this material other than for purposes permitted by law.

•Users may freely distribute the URL that is used to identify this publication.
•Users may download and/or print one copy of the publication from the University of Birmingham research portal for the purpose of private study or non-commercial research.
•User may use extracts from the document in line with the concept of 'fair dealing' under the Copyright, Designs and Patents Act 1988 (?)
•Users may not further distribute the material nor use it for the purposes of commercial gain.

Where a licence is displayed above, please note the terms and conditions of the licence govern your use of this document.

When citing, please reference the published version.

Take down policy
While the University of Birmingham exercises care and attention in making items available there are rare occasions when an item has been uploaded in error or has been deemed to be commercially or otherwise sensitive.

If you believe that this is the case for this document, please contact UBIRA@lists.bham.ac.uk providing details and we will remove access to the work immediately and investigate.

Download date: 05. May. 2023

This is an open access article published under a Creative Commons Attribution (CC-BY) License, which permits unrestricted use, distribution and reproduction in any medium, provided the author and source are cited.

Inorganic Chemistry

Article

pubs.acs.org/IC

Topotactic Fluorine Insertion into the Channels of $FeSb_2O_4$-Related Materials

Benjamin P. de Laune,[#] Gregory J. Rees,[§] José F. Marco,[†] Hien-Yoong Hah,[‡,⊥] Charles E. Johnson,[‡] Jacqueline A. Johnson,[‡,⊥] Frank J. Berry,[#] John V. Hanna,*[,§] and Colin Greaves*[,#]

[#]School of Chemistry, University of Birmingham, Birmingham B15 2TT, U.K.

[§]Department of Physics, University of Warwick, Coventry CV4 7AL, U.K.

[†]Instituto de Quimica-Fisica "Rocasolano", CSIC, Serrano 119, 28006 Madrid, Spain

[⊥]Department of Mechanical, Aeronautical and Biomedical Engineering and [‡]Center for Laser Applications, University of Tennessee Space Institute, Tullahoma, Tennessee 37388, United States

ABSTRACT: This paper discusses the fluorination characteristics of phases related to $FeSb_2O_4$, by reporting the results of a detailed study of $Mg_{0.50}Fe_{0.50}Sb_2O_4$ and $Co_{0.50}Fe_{0.50}Sb_2O_4$. Reaction with fluorine gas at low temperatures (typically 230 °C) results in topotactic insertion of fluorine into the channels, which are an inherent feature of the structure. Neutron powder diffraction and solid state NMR studies show that the interstitial fluoride ions are bonded to antimony within the channel walls to form Sb−F−Sb bridges. To date, these reactions have been observed only when Fe^{2+} ions are present within the chains of edge-linked octahedra (FeO_6 in $FeSb_2O_4$) that form the structural channels. Oxidation of Fe^{2+} to Fe^{3+} is primarily responsible for balancing the increased negative charge associated with the presence of the fluoride ions within the channels. For the two phases studied, the creation of Fe^{3+} ions within the chains of octahedra modify the magnetic exchange interactions to change the ground-state magnetic symmetry to C-type magnetic order in contrast to the A-type order observed for the unfluorinated oxide parents.

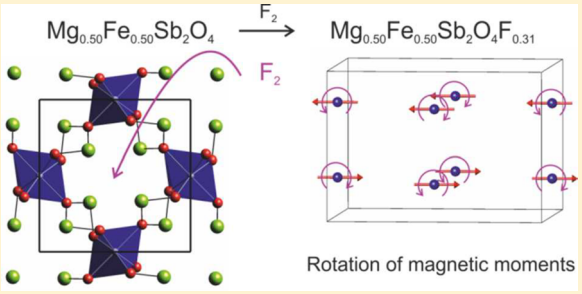

1. INTRODUCTION

Fluorine insertion into low-dimensional oxides is well understood and results in changes in structural properties, e.g., increased separation in layered materials, and electronic characteristics that are associated with oxidation of transition metal ions present in the parent material. These reactions have recently been reviewed,[1] and a classic example is provided by the conversion of semiconducting La_2CuO_4 to superconducting $La_2CuO_4F_x$ by heating in ambient pressure fluorine gas.[2] Similar reactions may also be observed for oxygen insertion, albeit generally at elevated pressures. We have recently reported[3] that phases related to $FeSb_2O_4$ (the mineral schafarzikite) can accommodate oxygen into the narrow one-dimensional channels that are an inherent feature of their structure. We have therefore examined whether related fluorine insertion reactions are possible. In this paper we report that this is, indeed, the case; we describe the nature of the redox reactions involved and compare the different anion insertion processes.

The structure of $FeSb_2O_4$ is tetragonal ($P4_2/mbc$ a = 8.62 Å c = 5.91 Å)[4] and contains chains of edge-sharing $Fe^{2+}O_6$ octahedra that are linked by trigonal pyramidal Sb^{3+} ions. The Sb^{3+} coordination becomes pseudotetrahedral if we include the lone pair of electrons (e) in the coordination geometry, SbO_3e. The combination of these structural features provides parallel channels (along the c-axis) into which the Sb^{3+} lone pairs of electrons are directed (Figure 1). The schafarzikite family, which can be represented by MSb_2O_4, is quite broad, and the members with M = Co[5] and M = Mg[6] are relevant to the present study. There have been several reports of the magnetic properties where M is a magnetic ion, especially of how elemental substitutions affect the magnetic exchange

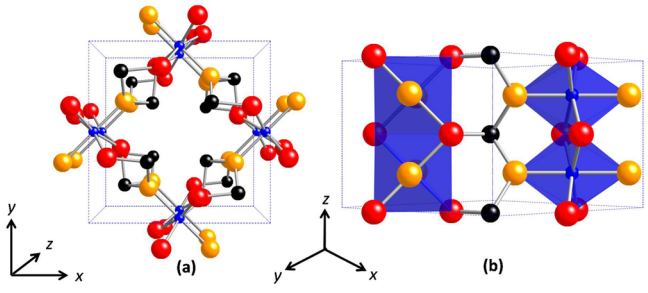

Figure 1. Structure of $FeSb_2O_4$ viewed along [001] (a), and [110] (b). Elements are shown as hard spheres—Fe (blue), Sb (black), apical oxygen (yellow), equatorial oxygen (red)—and their coordination environments are shown.

Received: June 28, 2017
Published: August 4, 2017

 © 2017 American Chemical Society

DOI: 10.1021/acs.inorgchem.7b01613
Inorg. Chem. 2017, 56, 10078−10089

interactions and thereby influence the nature of the low-temperature magnetic order.[5,7−10] All Sb-based materials which order magnetically at low temperatures have been found to display either A- or C-type modes of order with the moments aligned perpendicular to [001] or along [001], as shown in Figure 2. $FeSb_2O_4$, for example, has A-type order below a Néel

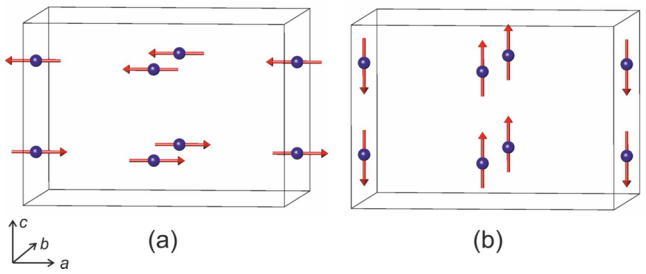

Figure 2. Two commonly observed spin alignments in magnetically ordered schafarzikite-related materials: (a) A-type with moments perpendicular to [001] and (b) C-type with moments along [001].

temperature, T_N = 45 K,[11] whereas $CoSb_2O_4$ is C-type with T_N = 79 K.[5] Interestingly, partial oxidation of Fe^{2+} to Fe^{3+} via cation substitution, $FeSb_{2-x}Pb_xO_4$,[8] or in oxygen-excess phases, e.g., $Mg_{0.50}Fe_{0.50}Sb_2O_{4+x}$,[12] cause a switch from A-type to C-type order. However, the pure Fe^{3+} compound $FePbBiO_4$ is A-type,[13] which highlights the delicate balance that exists between the intrachain and interchain magnetic exchange interactions and how small changes to the relative magnitudes of direct and superexchange magnetic interactions within the chains of octahedra influence the three-dimensional (3-D) magnetic order. The only reports of electronic conductivity relate to Fe^{2+}-containing phases and suggest semiconductor behavior with higher conductivities being observed for materials containing mixed Fe^{2+}/Fe^{3+} compositions.[3,8]

We have recently reported that unusual oxidation reactions can occur in air or oxygen with retention of the basic structure.[3,12] The reactions occur at low temperatures, e.g., at 350 °C, but it has been seen only for compounds which contain some Fe^{2+} cations. The reaction involves insertion of oxide ions into the empty channels, with charge balance being provided by simultaneous oxidation of Fe^{2+} ions to Fe^{3+} and Sb^{3+} to Sb^{5+}. The stability appears to be enhanced by the formation of defect clusters in the channels: these contain two 4-coordinate Sb^{3+}, two interstitial O^{2-} ions, and one 5-coordinate Sb^{5+}.[3] High levels of oxygen insertion occur when the Fe^{2+} concentration is high, e.g., in $FeSb_2O_4$, and this causes structural strain and broadening of diffraction peaks. However, this is not apparent for compounds such as $Fe_{0.50}Mg_{0.50}Sb_2O_4$, for which detailed investigations are possible.

These low temperature oxidations are of interest for their demonstration that the schafarzikite structure may be useful for materials with relevant electrocatalytic and ion transport properties. Given the high oxidation potential of fluorine gas, we have studied its low temperature reactions with Fe^{2+}-containing schafarzikite phases and compared the nature of the reactions with those reported previously for the production of oxygen-excess phases.[3,12] Here we report a detailed study of two representative materials, $Mg_{0.50}Fe_{0.50}Sb_2O_4$ and $Co_{0.50}Fe_{0.50}Sb_2O_4$. We show that similar reactions occur, but the Sb−F bonding preferences are different from Sb−O and result in significant differences not only to the structural characteristics, but also to the nature of the redox processes involved.

2. EXPERIMENTAL DETAILS

Parent materials were prepared by heating dried mixed metal oxides and antimony metal (CoO, 325 mesh Sigma-Aldrich; Fe_2O_3, ≥99.9% Sigma-Aldrich; Sb_2O_3, Reagent Plus, Sigma-Aldrich; Sb, BDH; MgO, ≥99% 325 mesh Sigma-Aldrich) in evacuated sealed quartz tubes as previously described.[7] Samples were fluorinated by heating in flowing F_2 (10% in N_2) at 230 °C for various times. After each heat treatment the reaction vessel was immediately purged with N_2 or Ar gas.

Powder X-ray diffraction (XRPD) analysis was performed on a Bruker D8 diffractometer in transmission geometry (monochromatic Cu−$K_{\alpha 1}$ radiation source, λ = 1.5406 Å). Neutron powder diffraction (NPD) data sets were collected (from samples of ca. 2−3 g in 8 mm vanadium cans) at 4 and 300 K on the diffractometer D2B at ILL, Grenoble, France. Data obtained from the central portion of the detector were used in the analysis to limit low angle asymmetry. Crystallographic and magnetic structure determinations were performed using the Rietveld method[14] and the general structures analysis system (GSAS)[15] and EXPGUI.[16] The magnetic refinements for 4 K data used form factors for Fe^{3+} and Co^{2+} based on evidence gained from the 300 K data and Mössbauer spectroscopy, which suggested that Fe^{3+} was the major iron species present. Magnetic properties were determined with an MPMS Quantum Design XL instrument: field-cooled (FC) and zero-field cooled (ZFC) measurements were taken with an applied field of 100 Oe. Thermogravimetric (TG) properties were investigated with a Netzsch Sta 449 F1 analyzer by heating samples at 10 K/min to 873 K in flowing 10% H_2 in N_2. The ^{57}Fe- and ^{121}Sb-Mössbauer spectra were recorded at 300 K with constant acceleration spectrometers using ^{57}Co/Rh and ^{121m}Sn sources. All spectra were computer fitted and the chemical isomer shift data are quoted relative to metallic iron at room temperature. The distribution of O^{2-} and F^- ions among the available anion sites was investigated using Madelung energy calculations.[17]

All solid state ^{19}F MAS NMR experiments were undertaken at 2.35 T (ν_0 ^{1}H = 100 MHz) using a modified Bruker Avance III HD spectrometer operating at a ^{19}F Larmor frequency of 94.2 MHz. Each measurement was performed using a dual channel Bruker HX 1.3 mm double-air-bearing MAS probe which enabled a MAS frequency of 50 kHz in all experiments. All ^{19}F MAS NMR data were acquired using a rotor-synchronized Hahn echo experiment ($\pi/2-4\tau-\pi-4\tau$) to record a full echo with only half echo processing being used which ensured that no broad components were distorted or lost in the experimental dead time after the $\pi/2$ pulse. A secondary solid PTFE reference (δ_{iso} = −123.4 ppm w.r.t. $CCl_3F_{(l)}$)[18,19] was used to determine a 1 μs $\pi/2$ excitation pulse, and to establish ^{19}F chemical shift referencing. A measured relaxation time of 0.1 s was determined, which is appropriate for the paramagnetic species and gave minimum saturation of any F_2 resonances present. The data were simulated and deconvoluted using the DMFit software package.[20]

3. RESULTS

3.1. Crystal and Magnetic Structure Determination.

The samples $Co_{0.50}Fe_{0.50}Sb_2O_4$ and $Mg_{0.50}Fe_{0.50}Sb_2O_4$ were selected for detailed study from a wide range of synthesized compounds, since they offered sufficient fluorine contents for reliable structure analysis while avoiding complications of broadened diffraction peaks seen for samples with higher iron contents; this also occurs for oxygen-excess phases as previously discussed.[3] XRPD data showed that the products of fluorination were single phase with structures closely related to that of the parent oxides; Figure 3 shows data for the formation of $Co_{0.50}Fe_{0.50}Sb_2O_4F_x$ from $Co_{0.50}Fe_{0.50}Sb_2O_4$.

3.1.1. Structure Analysis, 300 K. The structure was refined against NPD data in $P4_2/mbc$ using structural information from the related oxygen-excess phases[12] as a model for locating the

DOI: 10.1021/acs.inorgchem.7b01613
Inorg. Chem. 2017, 56, 10078−10089

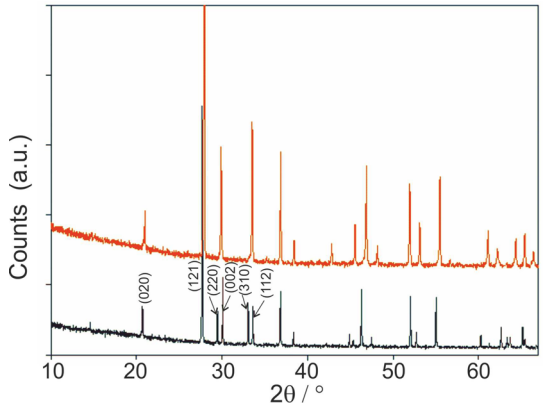

Figure 3. XRPD patterns showing how the structure of $Co_{0.50}Fe_{0.05}Sb_2O_4$ (black) changes upon fluorination to form $Co_{0.50}Fe_{0.50}Sb_2O_4F_x$ (red). The significant reflections for $2\theta < 35°$ are shown for $Co_{0.50}Fe_{0.05}Sb_2O_4$, and convergence of the (220)/(002) and (310)/(112) peaks occurs after fluorination.

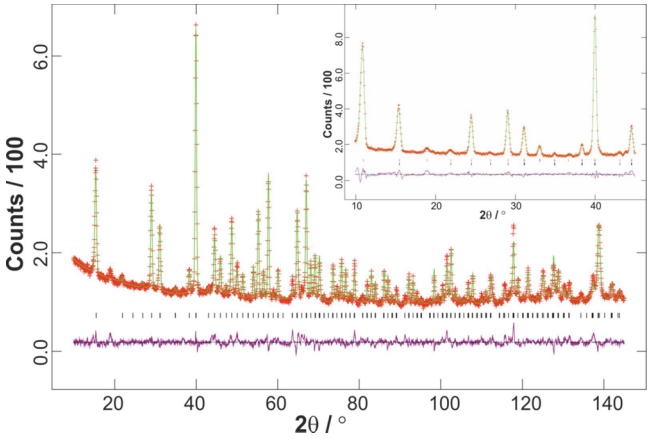

Figure 4. Rietveld refinement profiles for $Co_{0.50}Fe_{0.50}Sb_2O_4F_{0.49}$ showing raw data (red crosses), fitted profile (green), and difference profile (mauve). Reflection positions are marked as vertical bars: crystal structure (black), magnetic structure (red). The low angle region at 4 K is shown in the inset to highlight the magnetic scattering.

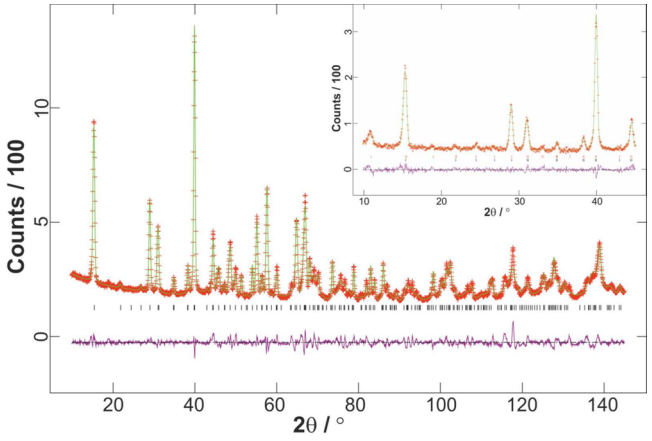

Figure 5. Rietveld refinement profiles for $Mg_{0.50}Fe_{0.50}Sb_2O_4F_{0.31}$ showing raw data (red crosses), fitted profile (green), and difference profile (mauve). Reflection positions are marked as vertical bars: crystal structure (black), magnetic structure (red). The low angle region at 4 K is shown in the inset to highlight the magnetic scattering.

interstitial fluorine. Satisfactory refinements were achieved for both materials and located interstitial fluorine within the channels at sites which are closely related to those reported for oxygen excess phases.[3,12] The isotropic displacement parameters for the fluorine and the two oxygen sites (equatorial, O_{eq}, and apical, O_{ap}, as shown in Figure 1) were constrained to be equal to limit correlation effects between the F site occupancy and its displacement parameter. The diffraction peaks for $Mg_{0.50}Fe_{0.50}Sb_2O_4F_x$ showed evidence for shoulders which were attributed to a non-homogeneous distribution of fluorine within the sample. Although fitting the data to two phases was possible, refinement using a single phase was more stable and was therefore adopted. After Rietveld refinement, the profile data are shown in Figures 4 and 5 and the structural data in Tables 1 and 2 for $Co_{0.50}Fe_{0.50}Sb_2O_4F_x$ and $Mg_{0.50}Fe_{0.50}Sb_2O_4F_x$, respectively. Since NPD cannot differentiate between oxygen and fluorine, Tables 1 and 2 assume that the inserted fluorine occupies the intrachannel site and does not undergo any substitution with framework O_{ap} or O_{eq} sites. Thermodynamic support for this anion distribution was sought using Madelung energy calculations,[17] which provide good relative stabilities for different ionic arrangements that are possible for a given material.

Madelung energies were computed based on the structural data for $Co_{0.50}Fe_{0.50}Sb_2O_4F_x$, Table 1, with a fluorine content of 0.5 per formula unit (in accordance with the site occupancies in Table 1) and charge balance via oxidation Fe^{2+} to Fe^{3+}. Structures were examined in which fluorine was allowed to substitute for both apical and equatorial oxide ions, and the results, Figure 6, revealed very little difference for substitution at O_{ap} and O_{eq} sites. An alternative charge balance involving a combination of Fe^{2+} and Sb^{3+} oxidation, suggested by Mössbauer spectroscopy (section 3.2), was also examined, and the results are included in Figure 6. The data provide no thermodynamic evidence to suggest any F/O exchange in the material, with fluorine showing a strong preference to remain in interstitial channel sites according to a higher Madelung energy of ~4%. However, it should be noted that the interstitial fluorine sites are occupied only to the extent of ~12%, and the model used distributes the charge evenly across all equivalent sites. This will result in a higher repulsive interaction between the channel sites than would occur in reality, where short-range order could avoid very close contacts between the anions. In the computations, this will destabilize structures with oxide ions in the channels more than those involving interstitial fluoride ions because of the higher ionic charge on oxygen. To evaluate the magnitude of this contribution, the structure was transformed to $P\bar{1}$ symmetry which allowed the selection of two well-separated positions for the two interstitial anions in the unit cell (to give the required composition). This model slightly increased the stability of all distributions, but especially those with oxygen within the channels, as expected. In all cases, however, the Madelung energy for fluorine occupancy of the channels remained >1.3% higher than for fluorine occupancy of framework sites (O_{ap} or O_{eq}) and confirmed the structural assignments in Tables 1 and 2.

Table 3 compares some relevant bond distances for the starting materials with those in the fluorinated products and some common trends are seen. The bond distances around the octahedral cations decrease on fluorination which is consistent with oxidation of some Fe^{2+} ions to Fe^{3+}. The higher charge provides enhanced cation−cation repulsions within the chains of octahedra, which is reflected in the increased *c*-parameter

DOI: 10.1021/acs.inorgchem.7b01613
Inorg. Chem. 2017, 56, 10078−10089

Table 1. Results of Rietveld Refinement against NPD data at 300 and 4 K (data in Italics) for $Co_{0.50}Fe_{0.50}Sb_2O_4F_x$[a]

atom	position	x	y	z	100 × U_{iso}/Å^2	occupancy
Co/Fe	4*d*	0	0.5	0.25	1.34(8)	0.5/0.5
					0.94(7)	
Sb	8*h*	0.1660(5)	0.1634(5)	0	2.28(7)	1.0
		0.1662(5)	*0.1625(5)*		*1.80(6)*	
O_{ap}	8*g*	0.6747(3)	0.1747(3)	0.25	2.18(6)	1.0
		0.6739(3)	*0.1739(3)*		*1.73(5)*	
O_{eq}	8*h*	0.1000(4)	0.6348(4)	0	2.18(6)	1.0
		0.1000(4)	*0.6359(4)*		*1.73(5)*	
F	16*i*	0.555(3)	0.468(4)	0.268(4)	2.18(6)	0.120(4)
		0.560(2)	*0.474(3)*	*0.265(4)*	*1.73(5)*	*0.127(4)*

[a] *a* = 8.4270(3) (*8.4123(2)*) Å, *c* = 5.9501(2) (*5.9383(2)*) Å, $P4_2/mbc$. Magnetic moment for Co/Fe at 4 K: *3.58(5)* μ_B. χ^2 = 4.3 (6.1); R_{wp} = 0.038 (0.044); R_F^2 = 0.076 (0.090).

Table 2. Results of Rietveld Refinement against NPD data at 300 and 4 K (data in italics) for $Mg_{0.50}Fe_{0.50}Sb_2O_4F_x$[a]

atom	position	x	y	z	100 × U_{iso}/Å^2	occupancy
Mg/Fe	4*d*	0	0.5	0.25	0.98(7)	0.5/0.5
					0.29(8)	
Sb	8*h*	0.1671(6)	0.1649(6)	0	2.01(8)	1.0
		0.1660(6)	*0.1646(7)*		*1.14(8)*	
O_{ap}	8*g*	0.6766(3)	0.1766(3)	0.25	1.83(6)	1.0
		0.6766(4)	*0.1766(4)*		*1.10(7)*	
O_{eq}	8*h*	0.1003(4)	0.6335(5)	0	1.83(6)	1.0
		0.1005(5)	*0.6337(6)*		*1.10(7)*	
F	16*i*	0.559(4)	0.467(7)	0.250(7)	1.83(6)	0.077(4)
		0.561(5)	*0.454(6)*	*0.247(7)*	*1.10(7)*	*0.080(4)*

[a] *a* = 8.4537(6) (*8.4410(8)*) Å, *c* = 5.9451(3) (*5.9353(3)*) Å, $P4_2/mbc$. Magnetic moment for Fe at 4 K: *2.5(1)* μ_B. χ^2 = 10.6 (6.1); R_{wp} = 0.046 (0.044); R_F^2 = 0.048 (0.090).

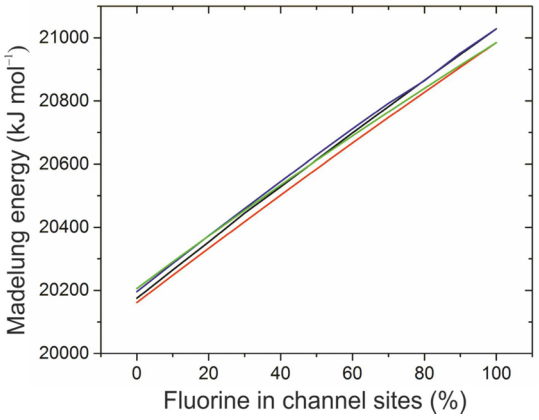

Figure 6. Variation of Madelung energy with percentage of fluorine occupying channel sites. Red line − F in O_{ap} sites with charge balance on Fe and Sb sites; black line − F in O_{ap} sites with charge balance on only Fe sites; blue line − F in O_{eq} sites with charge balance on only Fe sites; green line − F in O_{eq} sites with charge balance on Fe and Sb sites.

and automatically the larger cation−cation distance between adjacent cations. We also see that fluorination causes an increase in the averaged Sb−O bond lengths, which is consistent with some of the Sb ions increasing their coordination by bonding to an interstitial fluoride ion. It is interesting that the bridging bonds between F and two Sb ions have slightly different lengths. However, there is no special space group position that would constrain the bonds to be equal, and the fluorine position reflects not only the bonding to the two Sb ions, but also more distant structural aspects. Detailed bond distance comparisons around the Sb ions is not possible because we have only average bond distances, and these reflect ions with coordination numbers of 3 and 4.

The mean site occupancies from 300 and 4 K data (see below) refinements suggest compositions of $Co_{0.50}Fe_{0.50}Sb_2O_4F_{0.49(2)}$ and $Mg_{0.50}Fe_{0.50}Sb_2O_4F_{0.31(2)}$. These compositions will be used to describe the fluorinated phases throughout this paper. The difference in fluorine content in these samples probably relates to differences in particle size for the starting materials. Because of this, the fluorinating conditions were not identical. The compositions can be compared with the fluorine content of 0.50 per formula unit if oxidation of all Fe^{2+} to Fe^{3+} occurred completely and was the only charge balance mechanism for the interstitial fluorine. The concentration of interstitial anions is therefore compatible with oxidation of only Fe^{2+}, whereas for the analogous oxygen insertion reactions, oxidation of both Fe^{2+} and Sb^{3+} cations was necessary to explain the significantly higher concentrations of anions in the channels.[12] The results from Mössbauer spectroscopy, section 3.2, address this question.

Figure 7 compares the interstitial F atom positions for $Co_{0.50}Fe_{0.50}Sb_2O_4F_{0.49}$ (Table 1) with the O positions in $FeSb_{1.25}Pb_{0.75}O_{4.24}$.[8] The data for $Mg_{0.50}Fe_{0.50}Sb_2O_4F_{0.31}$ and $Co_{0.50}Fe_{0.50}Sb_2O_4F_{0.49}$ are very similar as indicated by Table 3, which compares important bond distances for the starting materials and fluorinated products; common trends are seen for both systems. For both O and F insertion, the anion is bonded to two Sb ions, which are at z = 0 and 0.5 for an anion at $z \approx$ 0.25, but the arrangements are slightly different: the Sb−F distances are longer than those for Sb − O, which pushes the F ions toward the center of the channel. The two Sb−F distances

DOI: 10.1021/acs.inorgchem.7b01613
Inorg. Chem. 2017, 56, 10078−10089

Table 3. Selected Bond Distances (Å) for $Co_{0.50}Fe_{0.50}Sb_2O_4F_{0.49}$ and $Mg_{0.50}Fe_{0.50}Sb_2O_4F_{0.31}$ at 300 K

	$Co_{0.50}Fe_{0.50}Sb_2O_4$ [ref 7]	$Co_{0.50}Fe_{0.50}Sb_2O_4F_{0.49}$	$Mg_{0.50}Fe_{0.05}Sb_2O_4$	$Mg_{0.50}Fe_{0.50}Sb_2O_4F_{0.31}$
Co/Fe/Mg−O_{ap} [×2]	2.165(1)	2.083(4)	2.151(1)	2.111(4)
Co/Fe/Mg−O_{eq} [×4]	2.0808(9)	2.052(3)	2.075(1)	2.050(3)
Fe−Fe	2.95921(5)	2.9750(1)	2.96139(9)	2.9726(1)
Sb−O_{ap} [×2]	1.993(1)	2.020(3)	2.000(1)	2.003(4)
Sb−O_{eq}	1.947(2)	1.987(6)	1.933(2)	1.985(6)
Sb−F		2.15(2)		2.07(4)
		2.35(3)		2.43(6)

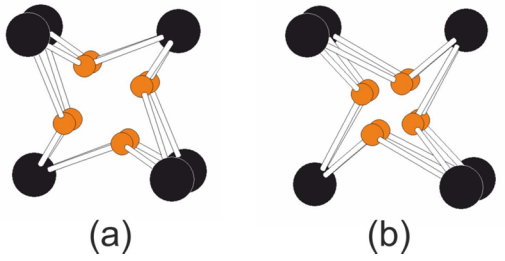

Figure 7. Interstitial O atom positions in $FeSb_{1.25}Pb_{0.75}O_{4.24}$[8] (a), compared with the F atom positions in $Co_{0.50}Fe_{0.50}Sb_2O_4F_{0.49}$ (Table 1) (b). All partially occupied sites are shown.

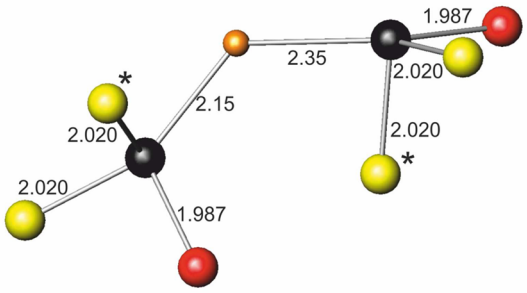

Figure 8. Interstitial F (orange) bridging two Sb ions (black) viewed approximately along [111] and showing bonds distances in Å. O_{ap} and O_{eq} ions are shown in yellow and red, respectively. The ions marked * are opposite the position of the lone pairs of electrons on Sb.

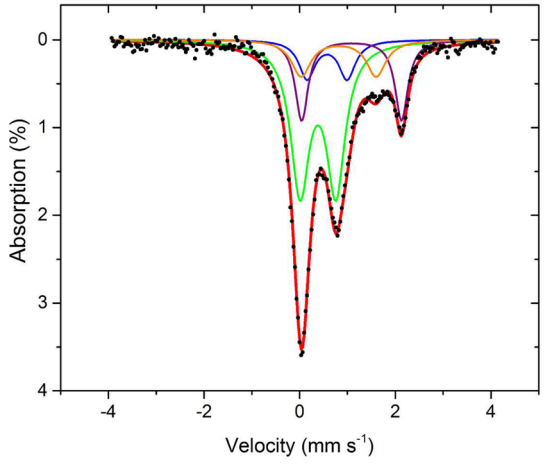

Figure 9. ^{57}Fe Mössbauer spectrum from $Mg_{0.50}Fe_{0.50}Sb_2O_4F_{0.31}$ at 300 K: observed data (black points), Fe^{2+} (purple and orange), Fe^{3+} (green and blue), overall (red).

are not equal, and the Sb−O distances have increased in length after the fluorination; this is consistent with an increase in

Table 4. ^{57}Fe Mössbauer Parameters Recorded at 300 K from Fluorinated Derivatives of $Co_{0.50}Fe_{0.50}Sb_2O_4$ and $Mg_{0.50}Fe_{0.50}Sb_2O_4$

	assignment	IS ± 0.05 mm s^{-1}	QS ± 0.05 mm s^{-1}	spectral area/%
$Co_{0.50}Fe_{0.50}Sb_2O_4F_x$	Fe^{2+} (1)	1.16	1.91	19
	Fe^{2+} (2)	0.82	1.51	13
	Fe^{3+} (1)	0.50	0.90	16
	Fe^{3+} (2)	0.38	0.70	52
$Mg_{0.50}Fe_{0.50}Sb_2O_4F_x$	Fe^{2+} (1)	1.09	2.09	20
	Fe^{2+} (2)	0.82	1.60	14
	Fe^{3+} (1)	0.57	0.84	12
	Fe^{3+} (2)	0.38	0.75	54

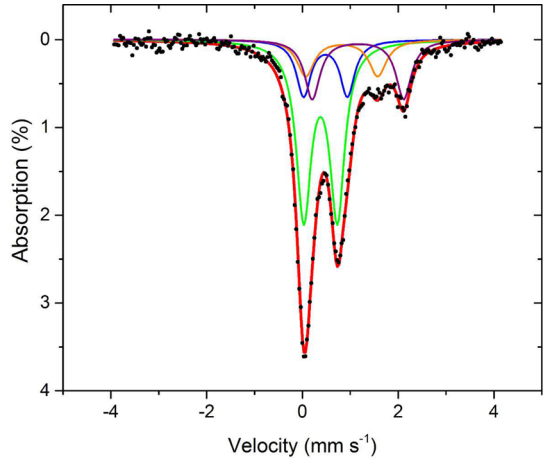

Figure 10. ^{57}Fe Mössbauer spectrum from $Co_{0.50}Fe_{0.50}Sb_2O_4F_{0.49}$ at 300 K: observed data (black points), Fe^{2+} (purple and orange), Fe^{3+} (green and blue), overall (red).

average coordination for Sb, but provides no support for any significant oxidation to Sb^{5+}. This structural aspect is explored later in section 3.2. The F-bridging between two Sb^{3+} cations is shown in Figure 8. It is interesting that the bridging bonds between F and two Sb ions have slightly different lengths. However, there is no special space group position that would constrain the bonds to be equal, and the fluorine position reflects not only the bonding to the two Sb ions, but also more distant structural aspects. Figure 8 shows that the fluorine bonds in such a way as to provide space for the Sb^{3+} lone pair of electrons, which are directed into the channels. The SbO_3eF coordination (e = lone pair) can be related to pseudo-D_{3h} symmetry where one of the two O_{ap} ions (marked * in Figure 8) and the lone pair lie on the C_3 axis, on opposite sides of the Sb ion. Detailed bond distance comparisons around the Sb ions are not possible unfortunately because the experimental distances are averages for ions with coordination numbers of

DOI: 10.1021/acs.inorgchem.7b01613
Inorg. Chem. 2017, 56, 10078−10089

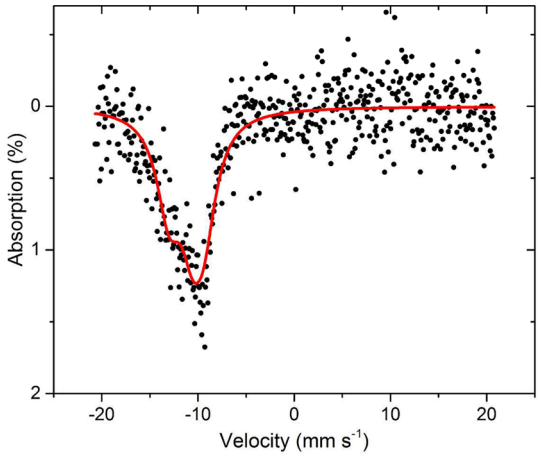

Figure 11. ^{121}Sb Mössbauer spectra from $Mg_{0.50}Fe_{0.50}Sb_2O_4F_{0.31}$ at 300 K showing fitting of observed data (black) to a single Sb^{3+} absorption (red).

Table 5. ^{121}Sb Mössbauer Parameters Recorded from Fluorinated Derivatives of $Co_{0.50}Fe_{0.50}Sb_2O_4$ and $Mg_{0.50}Fe_{0.50}Sb_2O_4$

	assignment	IS ± 0.15 mm s^{-1}	QS ± 0.15 mm s^{-1}	spectral area/%
$Co_{0.50}Fe_{0.50}Sb_2O_4F_x$	Sb^{3+}	−12.6	+7.54	95
	Sb^{5+}	0.03		5
$Mg_{0.50}Fe_{0.50}Sb_2O_4F_x$	Sb^{3+}	−10.94	+7.35	100

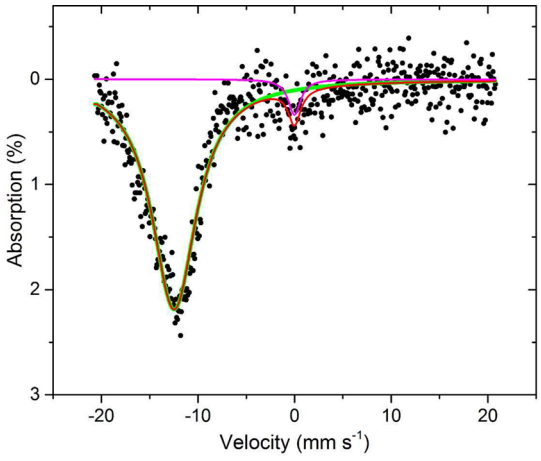

Figure 12. ^{121}Sb Mössbauer spectrum from $Co_{0.50}Fe_{0.50}Sb_2O_4F_{0.49}$ at 300 K: the data (black) are fitted to Sb^{3+} (green) and Sb^{5+} (cyan) to give the calculated profile (red).

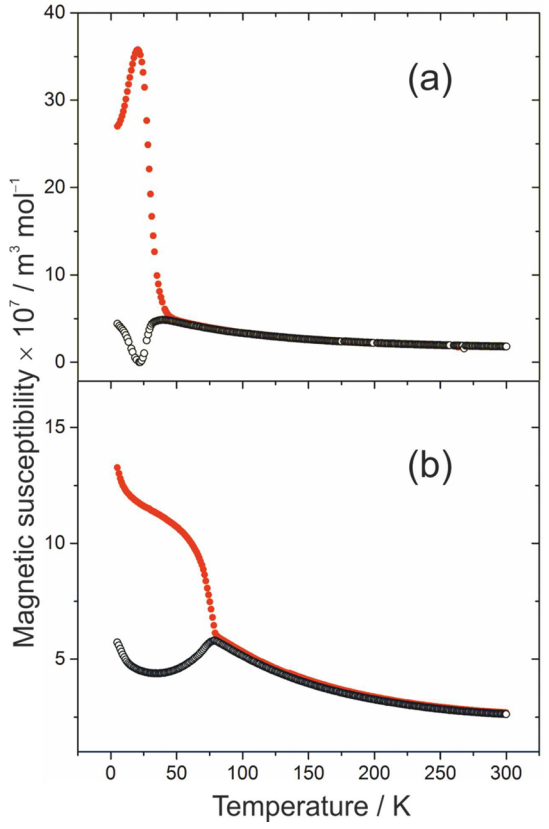

Figure 13. Magnetic susceptibility data (FC red, ZFC black) for (a) $Mg_{0.50}Fe_{0.50}Sb_2O_4F_{0.31}$ and (b) $Co_{0.50}Fe_{0.50}Sb_2O_4F_{0.49}$.

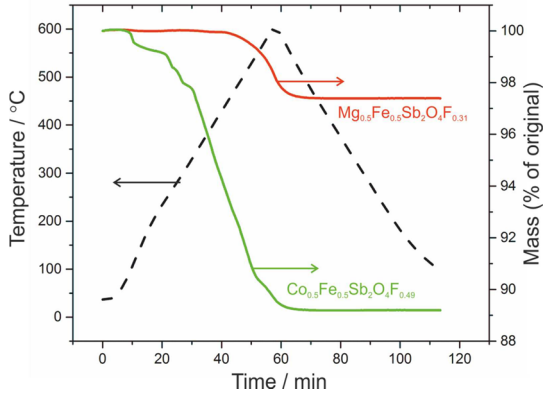

Figure 14. TG reduction of $Mg_{0.50}Fe_{0.50}Sb_2O_4F_{0.31}$ and $Co_{0.50}Fe_{0.50}Sb_2O_4F_{0.49}$ (compositions from NPD analysis) in 10% H_2 in N_2.

3 and 4. The bond distances around the octahedral cations decrease on fluorination which is consistent with oxidation of some Fe^{2+} ions to Fe^{3+}. The charge increase provides enhanced cation−cation repulsions along the chains of octahedra and is reflected in the increased *c*-parameter and hence the larger cation−cation distance between adjacent cations.

3.1.2. Magnetic Structure, 4 K. Magnetic structures were refined by introducing a discrete magnetic-only phase with *P*1 symmetry to allow total flexibility in determining the magnetic order; lattice parameters for this cell were constrained to correspond with the nuclear cell. It was clear from the intense (100) peak at ca. 10.8°2θ (Figures 4 and 5) that the dominant type of magnetic order for both fluorinated phases was consistent with C-type (Figure 2), with ferromagnetic order along a given chain of octahedra and antiferromagnetic order between adjacent chains. This contrasts with the predominant A-type arrangement seen in both starting phases[7,12] and suggests significant oxidation of Fe^{2+} to Fe^{3+}. In fact, $Co_{0.50}Fe_{0.50}Sb_2O_4$ has a ground-state comprising a minor C-type component (35%) which corresponds to a rotation of the magnetic moments through ~30°.[7] Refinements proceeded smoothly to yield magnetic moments of 3.58(5) μ_B and 2.5(1) μ_B per transition metal for the Co and Mg variants, respectively. Small peaks at ca. 18.5°2θ can be seen in the diffraction patterns for both compounds at 300 and 4 K. These were assigned to a strong magnetic peak which is characteristic of

DOI: 10.1021/acs.inorgchem.7b01613
Inorg. Chem. 2017, 56, 10078−10089

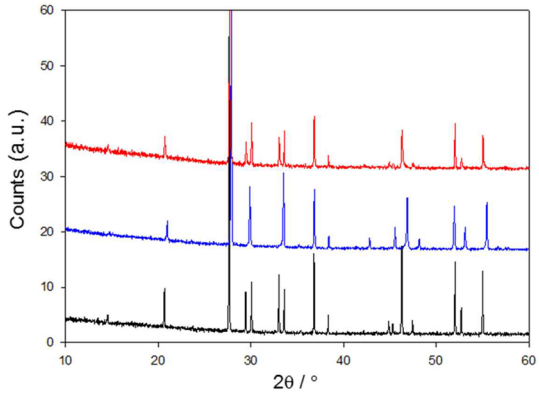

Figure 15. XRPD patterns for $Co_{0.50}Fe_{0.50}Sb_2O_4$ parent (black), $Co_{0.50}Fe_{0.50}Sb_2O_4F_{0.49}$ (blue), and $Co_{0.50}Fe_{0.50}Sb_2O_4$ after reduction of $Co_{0.50}Fe_{0.50}Sb_2O_4F_{0.49}$ in hydrogen (red).

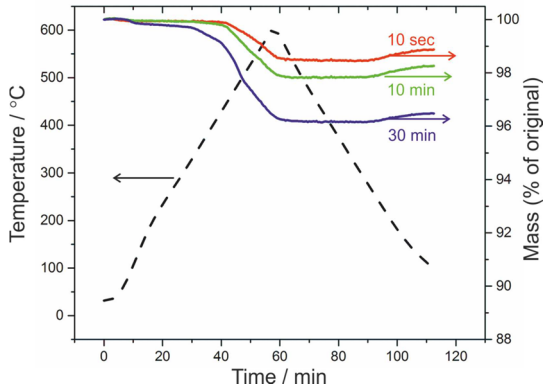

Figure 16. TG reduction (10% H_2 in N_2) of $Co_{0.50}Fe_{0.50}Sb_2O_4F_x$ samples formed by heating in fluorine gas for the indicated periods.

Table 6. Fluorine Contents Implied by Reductive TG Analysis for Samples of $Co_{0.50}Fe_{0.50}Sb_2O_4$ Heated under Flowing Fluorine Gas (230 °C) for Three Different Time Periods

time heated in F_2	% mass loss	implied fluorine content
~10 s	1.49	0.29
10 min	2.12	0.42
30 min	3.67	0.73

spinel phases; these are presumed to be very small amounts of $(Co,Fe)_3O_4$ and $(Mg,Fe)_3O_4$.

Assuming full conversion of Fe^{2+} to Fe^{3+}, the theoretical spin-only moments for the transition metal ions relevant to NPD data are 4.0 μ_B and 5.0 μ_B for $Co_{0.50}Fe_{0.50}Sb_2O_4F_{0.49}$ and $Mg_{0.50}Fe_{0.50}Sb_2O_4F_{0.31}$, respectively. Given the high orbital contribution inherent in Co^{2+} ions, the experimental moments are therefore smaller than expected, especially for $Mg_{0.50}Fe_{0.50}Sb_2O_4F_{0.31}$. It is important to recognize that this effect appears to be a feature of phases of this type with mixed cations on the octahedral sites, and moments for $Co_{0.50}Fe_{0.50}Sb_2O_4$ and $Mg_{0.50}Fe_{0.50}Sb_2O_4$ have been reported to be 2.12(4) and 2.24(5) μ_B,[7,12] respectively, compared with spin-only values of 3.5 and 4.0 μ_B per transition metal ion. This has previously been attributed to the effects of disorder within the chains of octahedra and the similarity in exchange interactions for A- and C-type order, such that some magnetic ions show no long-range magnetic order; this has been supported by the results of Mössbauer spectroscopy.[12]

It is interesting that both oxygen and fluorine insertion reactions result in stabilization of the C-type magnetic structure. In the starting materials, the diamagnetic Mg^{2+} ions weaken the magnetic exchange interactions,[12] whereas Co^{2+} stabilizes the C-type structure relative to A.[7] These effects will also be apparent in the fluorinated products. It is likely that the effects of oxidation of Fe^{2+} to Fe^{3+} are more important to intrachain magnetic exchange rather than to interchain effects. Two significant interactions occur within the chains: direct exchange involving t_{2g} orbital overlap and ~90° superexchange involving the oxygen ions forming the common edges of the linked octahedra. It is difficult to predict, *a priori*, the results of oxidation because of conflicting effects. Direct exchange (favoring antiferromagnetic order within each chain and therefore A-type order) would be enhanced by the maximum number of half-filled t_{2g} orbitals on Fe^{3+} ions, but reduced by the increased separation between adjacent cations within each chain (caused by the increased cation−cation repulsions and reflected in the *c* unit cell parameter). Enhanced covalence and the d^5 Fe^{3+} configuration should increase the superexchange which favors ferromagnetic order within each chain and overall C-type order. The latter effect seems to be dominant, at least for the materials examined to date.

3.2. Mössbauer Spectroscopy. The ^{57}Fe- and ^{121}Sb-Mössbauer spectra recorded from $FeSb_2O_4$ showed components characteristic of Fe^{2+} and Sb^{3+}.[21] Fluorination of both $Mg_{0.50}Fe_{0.50}Sb_2O_4$ and $Co_{0.50}Fe_{0.50}Sb_2O_4$ gave materials from which the ^{57}Fe- and ^{121}Sb-Mössbauer spectra showed that Fe^{2+} had been largely oxidized to Fe^{3+}, whereas Sb^{3+} showed little signs of oxidation. The spectrum recorded from fluorinated $Mg_{0.50}Fe_{0.50}Sb_2O_4F_{0.31}$ is shown in Figure 9 and ^{57}Fe Mössbauer parameters are collected in Table 4. The results show that, upon fluorination, ca. 66% of the Fe^{2+} in the pure oxide is oxidized to Fe^{3+}. This agrees well with the NPD data, which show the bulk material to contain 62% Fe^{3+}, assuming no oxidation of Sb^{3+} ions. The Fe^{3+} and Fe^{2+} components were both amenable to fitting to more than one site and are designated here as $Fe^{2+}(1)$, $Fe^{2+}(2)$, $Fe^{3+}(1)$, $Fe^{3+}(2)$. This fitting is attributed to the best approximation to the variety of local sites experienced by the octahedral cations that result from an essentially random arrangement within the chains and also more distant effects of the partially occupied fluorine sites. The Fe^{2+} and Fe^{3+} components are typical for an oxide environment and provide no evidence that fluorine may occupy sites within the structural framework.

The ^{57}Fe Mössbauer results from $Co_{0.50}Fe_{0.50}Sb_2O_4F_{0.49}$ (Figure 10, Table 4) are similar to those from $Mg_{0.50}Fe_{0.50}Sb_2O_4F_{0.31}$ and demonstrate that fluorination induces ca. 68% of Fe^{2+} in the pure oxide to be oxidized to Fe^{3+}, sufficient to compensate for 0.34F. The spectra also show two components for each of Fe^{2+} and Fe^{3+} species with isomer shifts similar to those recorded from $Mg_{0.50}Fe_{0.50}Sb_2O_4F_{0.31}$.

The ^{121}Sb Mössbauer results (Figure 11, Table 5) from $Mg_{0.50}Fe_{0.50}Sb_2O_4F_{0.31}$ show a single resonance (IS = −10.9 mm s^{-1}) consistent with only Sb^{3+} and thereby confirming that oxidation of antimony is insignificant for this material. The broad nature of the line width (ca. 4 mm s^{-1}) may suggest more than one environment for Sb^{3+} ions, which would be expected for bonding of some to the inserted F ions. However, in this study a single asymmetric peak was modeled by incorporating a quadrupole splitting. In contrast, the broad

DOI: 10.1021/acs.inorgchem.7b01613
Inorg. Chem. 2017, 56, 10078−10089

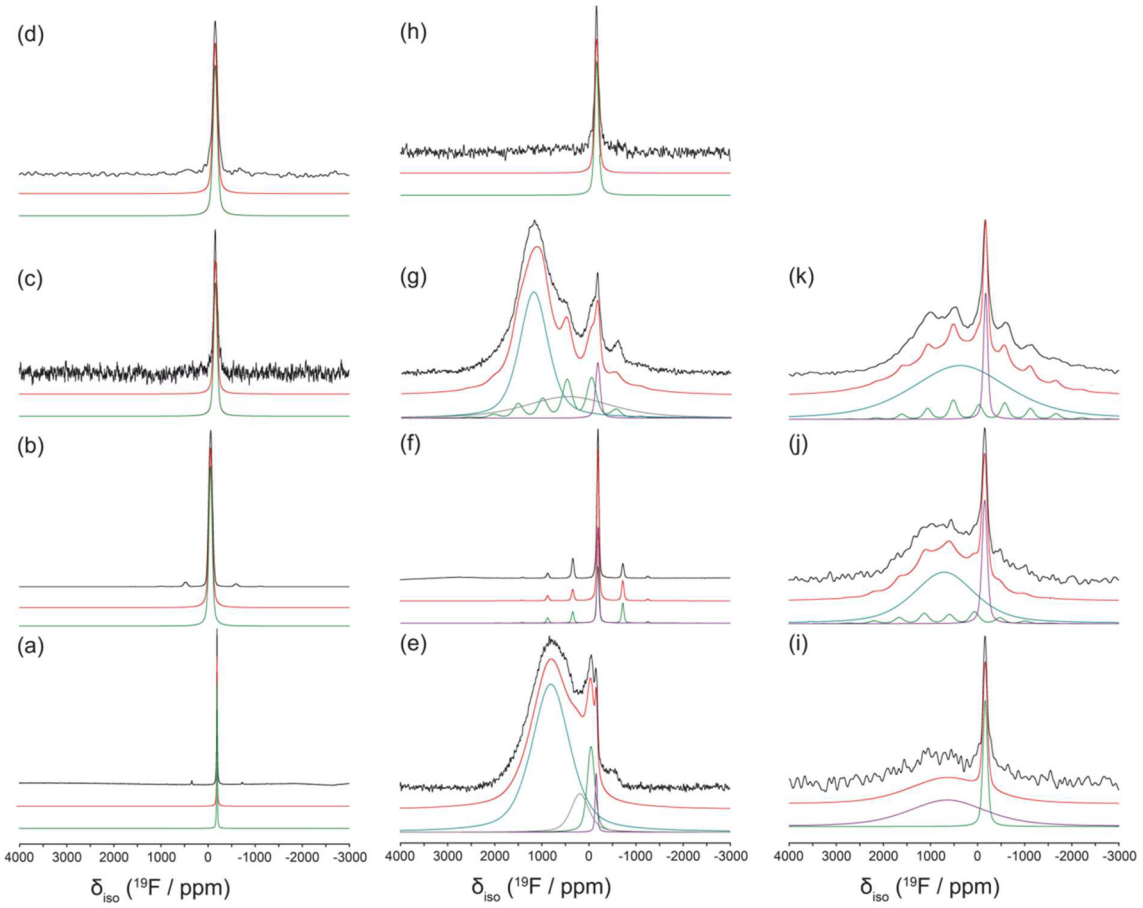

Figure 17. Solid state ^{19}F MAS NMR spectra of (a) MgF_2, (b) SbF_3, (c) FeF_2, (d) CoF_2, (e) $Mg_{0.50}Fe_{0.50}Sb_2O_4F_{0.31}$, (f) $Mg_{0.50}Fe_{0.50}Sb_2O_4F_{0.31}$ after TG reduction in H_2 at 600 °C, (g) $Co_{0.50}Fe_{0.50}Sb_2O_4F_{0.49}$, (h) $Co_{0.50}Fe_{0.50}Sb_2O_4F_x$ reduced on the TGA at 600 °C. The results of heating $Co_{0.50}Fe_{0.50}Sb_2O_4$ under flowing F_2 for varying time periods are shown in (i) 10 s, (j) 10 min, and (k) 30 min.

lined ^{121}Sb Mössbauer spectrum from $Co_{0.50}Fe_{0.50}Sb_2O_4F_{0.49}$ (Figure 12, Table 5) showed a small (ca. 5%) level of oxidation of Sb^{3+} to Sb^{5+}. This concentration of Sb^{5+} (0.1 Sb^{5+} per formula unit) corresponds to a fluorine content of 0.2, an overall fluorine content of 0.54, and composition of $Co_{0.50}Fe_{0.50}Sb_2O_4F_{0.54}$, in good agreement with the NPD analysis.

3.3. Magnetic Susceptibility. The magnetic susceptibilities of $Mg_{0.50}Fe_{0.50}Sb_2O_4F_{0.31}$ and $Co_{0.50}Fe_{0.50}Sb_2O_4F_{0.49}$ are plotted against temperature in Figure 13 and show that the oxidation of Fe^{2+} ions within the chains of octahedra results in a significant change in magnetic behavior. Both $Mg_{0.50}Fe_{0.50}Sb_2O_4F_{0.31}$ and $Co_{0.50}Fe_{0.50}Sb_2O_4F_{0.49}$ show canted antiferromagnetic transitions with T_N = 49(1) and 80 (1) K, respectively; these values can be compared with T_N = 20(2)[12] and 61(2)[7] K for the parent materials. The increased Néel temperatures indicate a strengthening in magnetic exchange interactions, not only within the chains (resulting in a change from A-type to C-type order) but also between the chains to provide the overall three-dimensional order. Unfortunately the materials do not show Curie–Weiss behavior and provide nonlinear plots of $(\text{susceptibility})^{-1}$ against temperature; this prevents reliable determination of effective moments or valid Weiss constants.

3.4. TG and Chemical Analysis. The fluorine content for a variety of materials was examined using a fluoride ion selective electrode after dissolution in HCl solutions. The results obtained indicated substantially higher fluorine contents than could be attributed to fluorine within the bulk material. It was therefore assumed that the samples contained significant, and variable, amounts of adsorbed and/or absorbed fluorine, and that the channels within the materials probably play a significant mechanistic role in this process.

TG analysis under reducing conditions (10% H_2 in N_2) was therefore explored in a further attempt to endorse the bulk fluorine contents deduced from crystallography and Mössbauer spectroscopy. Quantitative analysis of the decomposition products of oxide fluorides reduced in this way can often provide an accurate estimate of the fluorine content (see, for example, ref 22). Although this strategy could not address the bulk fluorine content in this study, it nevertheless provided some very interesting results. Figure 14 shows the mass losses from $Mg_{0.50}Fe_{0.50}Sb_2O_4F_{0.31}$ and $Co_{0.50}Fe_{0.50}Sb_2O_4F_{0.49}$ during heating to 600 °C. XRPD analysis of each reduced product, Figure 15, revealed only one crystalline phase, $Mg_{0.50}Fe_{0.50}Sb_2O_4$ and $Co_{0.50}Fe_{0.50}Sb_2O_4$, respectively. However, the mass losses associated with this reduction process were always larger than that expected from the NPD and Mössbauer spectroscopy data, and this was particularly pronounced for $Co_{0.50}Fe_{0.50}Sb_2O_4F_{0.49}$ and other materials studied containing cobalt. For example, the mass loss of 10.8% shown in Figure 14 for the cobalt containing phase studied in detail corresponds to the composition $Co_{0.50}Fe_{0.50}Sb_2O_4F_{2.1}$, which is unrealistic with respect to the

DOI: 10.1021/acs.inorgchem.7b01613
Inorg. Chem. 2017, 56, 10078–10089

Table 7. Deconvoluted Solid State ^{19}F MAS NMR Parameters for (a) MgF_2; (b) SbF_3; (c) FeF_2; (d) CoF_2; (e) $Mg_{0.50}Fe_{0.50}Sb_2O_4F_{0.31}$; (f) $Mg_{0.50}Fe_{0.50}Sb_2O_4F_{0.31}$ after TG reduction in H_2 at 600 °C; (g) $Co_{0.50}Fe_{0.50}Sb_2O_4F_{0.49}$; (h) $Co_{0.50}Fe_{0.50}Sb_2O_4F_{0.49}$ after TG reduction 600 °C[a]

	sample	peak	$\delta_{iso/para/cg}$ (ppm)	$\Delta\delta$[b] (ppm)	η[b]	intensity (%)
a	MgF_2	1	−198			100
b	SbF_3	1	−58			100
c	FeF_2	1	−163			100
d	CoF_2	1	−162			100
e	$Mg_{0.50}Fe_{0.50}Sb_2O_4F_{0.31}$	1	−165			2
		2	−50			9
		3	180			10
		4	800			79
f	$Mg_{0.50}Fe_{0.50}Sb_2O_4F_{0.31}$ after H_2 reduction	1	−197			45
		2	−190	1000	0	55
g	$Co_{0.50}Fe_{0.50}Sb_2O_4F_{0.49}$	1	−170			4
		2	450			25
		3	480	1473	0.4	18
		4	1190			53
h	$Co_{0.50}Fe_{0.50}Sb_2O_4F_{0.49}$ after H_2 reduction	1	−160			100
i	$Co_{0.50}Fe_{0.50}Sb_2O_4F_x$ 10 s. fluorination	1	−160			22
		2	640			78
j	$Co_{0.50}Fe_{0.50}Sb_2O_4F_x$ 10 min fluorination	1	−160			11
		2	590	1800	0.9	17
		3	700			72
k	$Co_{0.50}Fe_{0.50}Sb_2O_4F_x$ 30 min fluorination	1	−170			9
		2	590	1970	0.9	11
		3	370			80

[a]The NMR parameters for heating $Co_{0.50}Fe_{0.50}Sb_2O_4$ under flowing F_2 for varying time periods are given in i, j, and k. [b]Haeberlen shift convention: $|\delta_{33} - \delta_{iso}| \geq |\delta_{11} - \delta_{iso}| \geq |\delta_{22} - \delta_{iso}|$, $\delta_{iso} = (\delta_{11} + \delta_{22} + \delta_{33})/3$, $\Delta\delta = \delta_{33} - 1/2(\delta_{11} + \delta_{22}) = 3/2(\delta_{33} - \delta_{iso})$, $\eta_\delta = (\delta_{22} - \delta_{11})/(\delta_{33} - \delta_{iso})$ where $(1 \geq \eta_\delta \geq 0)$.

inserted fluorine. TG data therefore confirmed that fluorine atoms/ions were present in our samples in addition to the intrachannel fluoride ions. At first sight, it seems unusual that the fluorination reaction can be reversed under a hydrogen-rich atmosphere, but the reduction of Fe^{3+} to Fe^{2+} ions can certainly balance a feasible reaction, e.g.:

$$Co_{0.50}Fe_{0.50}Sb_2O_4F_{0.49} + 0.245H_2 \rightarrow Co_{0.50}Fe_{0.50}Sb_2O_4 + 0.49HF$$

HF molecules have the highest single bond energy, 567 kJ mol^{-1}, which is probably crucial in order to reverse the fluorination reaction and restore the initial oxide.

Some evidence was noticed for a possible correlation between the duration of a fluorination reaction and the amount of additional nonbulk fluorine suggested by TG measurements. In order to investigate this further, three samples were prepared from $Co_{0.50}Fe_{0.50}Sb_2O_4$ by heating under flowing F_2 for different lengths of time at 230 °C and then immediately conducting a reductive TG analysis (Figure 16). The TG results are given in Table 6; the samples were then included in a comprehensive solid state NMR investigation to reveal more information about the nature of fluorine in these oxide-fluoride compounds.

3.5. Solid State NMR. Although the NMR characteristics of ^{19}F have been exploited as probes for metal centers in paramagnetic bioinorganic NMR studies,[23] this study represents the first direct observation of paramagnetically influenced ^{19}F nuclei within solid state materials. The ^{19}F MAS NMR spectra of some binary fluorides (see Figure 17a–d) were measured as an aid to the interpretation of the more complex data acquired from $Mg_{0.50}Fe_{0.50}Sb_2O_4F_{0.31}$ (Figure 17e) and $Co_{0.50}Fe_{0.50}Sb_2O_4F_{0.49}$ (Figure 17g). These spectra exhibit an array of narrow and broad components spread over a large chemical shift range; this is the product of both the pseudocontact (electron–nuclear dipolar) shift and Fermi contact interactions, which together comprise the paramagnetic NMR shift interaction. As observed from Figure 17a–d and Table 7, the binary fluorides are characterized by single narrow resonances which fall within a ^{19}F chemical shift range of −58 to −198 ppm. The corresponding ^{19}F MAS NMR data from $Mg_{0.50}Fe_{0.50}Sb_2O_4F_{0.31}$ and $Co_{0.50}Fe_{0.50}Sb_2O_4F_{0.49}$ (see Figures 17, panels e and f, respectively) also exhibit narrow resonances with chemical shifts in this region; this corroborates the NPD data which conclusively shows that the F^- ions in the channels are bonded to Sb^{3+} ions. These resonances show distinct shoulders attributed to a small amount of chemical decomposition to form binary fluorides such as MgF_2, CoF_2, FeF_2, and SbF_3. In addition, the spectra of both fluorinated systems show two broad resonances representing a large distribution of F environments. For $Mg_{0.50}Fe_{0.50}Sb_2O_4F_{0.31}$, the broad component centered at $\delta_{cg} \approx 800$ ppm (Table 7) is assigned to the high (but variable) concentration of adsorbed/absorbed (possibly surface and intrachannel) fluorine in a paramagnetically shifted and disordered environment. It is interesting to note that after TG reduction at 600 °C (see Figure 17f), these broad resonances are not present, which supports the view that the resonance originates from the adsorbed/absorbed fluorine. The XRPD data of Figure 15 shows that the fluorine has been removed from the channels with no additional crystalline phases being formed. The narrower upfield resonances which possess a spinning sideband

DOI: 10.1021/acs.inorgchem.7b01613
Inorg. Chem. 2017, 56, 10078–10089

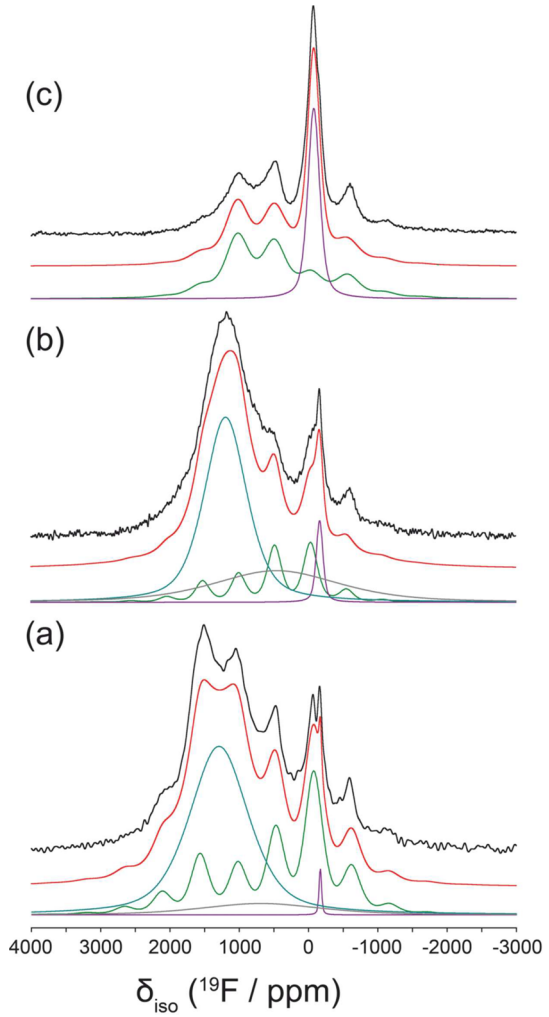

Figure 18. Solid state ^{19}F MAS NMR spectra and deconvolutions of (a) $Co_{0.25}Fe_{0.75}Sb_2O_4F_x$, (b) $Co_{0.5}Fe_{0.5}Sb_2O_4F_{0.49}$, and (c) $Co_{0.75}Fe_{0.25}Sb_2O_4F_x$.

Table 8. Deconvoluted Solid State ^{19}F MAS NMR Parameters for (a) $Co_{0.25}Fe_{0.75}Sb_2O_4F_x$, (b) $Co_{0.50}Fe_{0.50}Sb_2O_4F_x$ and (c) $Co_{0.75}Fe_{0.25}Sb_2O_4F_x$

	sample	peak	$\delta_{iso/para}$ (ppm)	$\Delta\delta^a$ (ppm)	η^a	intensity (%)
a	$Co_{0.25}Fe_{0.75}Sb_2O_4F_x$	1	−171			1
		2	470	1900	0.3	40
		3	686			7
		4	1291			52
b	$Co_{0.50}Fe_{0.50}Sb_2O_4F_x$	1	−169			4
		2	454			25
		3	482	1470	0.4	18
		4	1189			53
c	$Co_{0.75}Fe_{0.25}Sb_2O_4F_x$	1	−80	1540	0	65
		2	490			35

[a]Haeberlen shift convention: $|\delta_{33} - \delta_{iso}| \geq |\delta_{11} - \delta_{iso}| \geq |\delta_{22} - \delta_{iso}|$, $\delta_{iso} = (\delta_{11} + \delta_{22} + \delta_{33})/3$, $\Delta\delta = \delta_{33} - 1/2(\delta_{11} + \delta_{22}) = 3/2(\delta_{33} - \delta_{iso})$, $\eta_\delta = (\delta_{22} - \delta_{11})/(\delta_{33} - \delta_{iso})$ where $(1 \geq \eta_\delta \geq 0)$.

manifold must be from amorphous or small crystal size decomposition products formed by the channel Sb−F−Sb bridging species. A second "broad" component is required to complete the deconvolution of the spectrum shown in Figure 17e; this resonance at δ_{cg} = 180 ppm could be associated with the anisotropic behavior of the main broad resonance.

The ^{19}F MAS NMR data from $Co_{0.50}Fe_{0.50}Sb_2O_4F_{0.49}$ (see Figure 17g) can be deconvoluted in a similar fashion. Narrow resonances suggesting more ordered environments are observed at $\delta_{iso} \approx -170$ ppm, and these are assigned to the channel site, and possibly some contamination as occurs for $Mg_{0.50}Fe_{0.50}Sb_2O_4F_{0.31}$. Three broad resonances indicating more disordered fluorine environments are observed at $\delta_{cg} \approx 450$, 480, and 1190 ppm. The resonance centered at $\delta_{cg} \approx 450$ ppm is spread over the entire observed 5000 ppm paramagnetic shift range and appears to relate to an $F_{2(g)}$ environment possibly located at the surface. As observed in Figure 17h, the postreduction product formed under 10% H_2 in N_2 results in a single resonance at $\delta_{iso} \approx -160$ ppm and is assigned to poorly crystalline decomposition products CoF_2, FeF_2, and SbF_3.

The lack of resolution evident in ^{19}F MAS NMR data for the absorbed fluorine hinders the assignment of specific F environments. To assist with this problem, three samples were synthesized from the same parent $Co_{0.50}Fe_{0.50}Sb_2O_4$ by heating under flowing F_2 at 230 °C for different times (∼10 s, 10 min, and 30 min). These spectra are shown in Figure 17i−k, respectively. The initial addition of F_2 gives rise to two species characterized by a narrow ^{19}F resonance at ∼ −160 ppm and a broader ^{19}F resonance with a center of gravity at ∼640 ppm. The narrow resonance can be assigned to the channel site (and possibly a contaminant), while the broader resonance emanates from the additional adsorbed/absorbed fluorine. The exposure of the material to F_2 for 10 min increases the amount of the broad component and begins to show evidence of a third resonance, a paramagnetic shift anisotropic sideband manifold with a δ_{iso} = 590 ppm ($\Delta\delta$ = 1800 ppm, η = 0.90) (see Figure 17j). Upon further addition of F_2 up to 30 min, the intensity of the broad resonance increases further, and the sideband manifold of the third resonance becomes fully resolved (δ_{iso} = 590 ppm, $\Delta\delta$ = 1970 ppm, η = 0.90) (see Figure 17k). This resonance is attributed to absorbed fluorine, and the origin of the extensive sideband manifold is attributed to the electron−nuclear dipolar (pseudocontact) paramagnetic interacton arising from the fluorine being closer to the paramagnetic Co/Fe site, while the larger chemical shift can be accounted for by the Fermi contact hyperfine term.

A ^{19}F MAS NMR study focusing on the importance that Fe plays in the reaction with fluorine gas was undertaken by varying the Fe content (x) in the $Co_xFe_{1-x}Sb_2O_4F_y$ system (see Figure 18 and Table 8). As the Fe in the sample increases from $Co_{0.75}Fe_{0.25}Sb_2O_4F_y$ (Figure 18c) to $Co_{0.25}Fe_{0.75}Sb_2O_4F_y$ (Figure 18a), the percentage of the fluorine that is absorbed within the channels is observed to increase, as evidenced by the emerging dominance of the disordered resonance at δ_{cg} = 1200 ppm (Figure 18a,b). Hence, this experiment unambiguously demonstrates that the amount of fluorine absorbed into the channel structure, but not being chemically bonded to Sb, is strongly dependent on the Fe concentration in the initial oxide.

4. CONCLUSIONS

Phases related to $FeSb_2O_4$, and which contain some Fe^{2+} cations, have been shown to undergo topotactic fluorine insertion when heated at low temperatures in 10% F_2 in nitrogen. The fluorine occupies sites within the structural channels of the $FeSb_2O_4$ structure and forms bridges between two Sb^{3+} ions in a way that leaves space for the cation lone-pair of electrons to occupy a stereochemical position. The charges

DOI: 10.1021/acs.inorgchem.7b01613
Inorg. Chem. 2017, 56, 10078−10089

associated with the F^- ions are balanced primarily by oxidation of Fe^{2+} to Fe^{3+}, although a small amount of oxidation of Sb^{3+} to Sb^{5+} may also occur. Fluorination of $Mg_{0.50}Fe_{0.50}Sb_2O_4$ and $Co_{0.50}Fe_{0.50}Sb_2O_4$ was studied in detail and the fluorinated products order antiferromagnetically (T_N = 49(1) and 80(1) K, respectively) but with different magnetic ground states (C-type order) compared to their oxide parent phases (A-type order). This is attributed to a change in magnetic interactions resulting from the oxidation of Fe^{2+} to Fe^{3+}.

Characterization of the oxide-fluorides is hampered by the presence of significant fluorine in addition to that bonded to Sb in the channels. No evidence for this was indicated by NPD data, and it is assumed that the fluorine is adsorbed on surface sites or absorbed within the channels. This proposal was supported by the presence of a large ^{19}F MAS solid state NMR signal that indicated the presence of disordered fluorine. Fluorine contamination prevented reliable chemical analysis for the bulk fluorine content, which was necessarily based on NPD refined values. Reduction of the fluorinated materials under hydrogen removed not only the adsorbed/absorbed fluorine but also the channel fluorine. The phase is restored to its original state, although ^{19}F solid state NMR studies indicate that the channel fluorine probably remains in the material, and forms binary fluorides (amorphous or with very small crystal sizes) that will depend on the starting composition.

AUTHOR INFORMATION

Corresponding Authors

*(C.G.) E-mail: c.greaves@bham.ac.uk.

*(J.V.H.) E-mail: J.V.Hanna@warwick.ac.uk.

ORCID

Colin Greaves: 0000-0002-9568-3697

Notes

The authors declare no competing financial interest.

Data associated with the results shown in this paper are accessible from the University of Birmingham Archive: http://epapers.bham.ac.uk/3026/.

ACKNOWLEDGMENTS

We thank EPSRC for financial support of this research (EP/L014114/1) and also Spanish MINECO (Project MAT 2015-64110-C2-1-P). We are grateful to EPSRC, EU, and ILL for the provision of NPD facilities and we thank Dr. Emma Suard and Dr. Sarah Horswell for assistance in collecting the NPD data at ILL. The X-ray diffractometers TG analyser used in this research were obtained through Birmingham Science City: Creating and Characterising Next Generation Advanced Materials (West Midlands Centre for Advanced Materials Project 1), with support from Advantage West Midlands (AWM) and part funded by the European Regional Development Fund (ERDF). The Advanced Materials Facility is part of the Centre for Chemical and Materials Analysis in the School of Chemistry at the University of Birmingham. J.V.H. thanks the EPSRC, the University of Warwick and the Birmingham Science City Program for partial funding of the solid state NMR infrastructure at Warwick. The latter program accessed the Birmingham Science City Advanced Materials Project 1: Creating and Characterising Next Generation Advanced Materials, which derived support from Advantage West Midlands (AWM) and the European Regional Development Fund (ERDF).

REFERENCES

(1) Slater, P. R.; Driscoll, L. Modification of Magnetic and Electronic Properties, in Particular Superconductivity, by Low Temperature Insertion of Fluorine into Oxides. In *Photonic and Electronic Properties of Fluoride Materials*; Tressaud, A., Poppelmeier, K., Eds.; *Progress in Fluorine Science Series*; Elsevier: Amsterdam, 2016; Vol. *1*, pp 401−421.

(2) Chevalier, B.; Tressaud, A.; Lepine, B.; Amine, K.; Dance, J. M.; Lozano, L.; Hickey, E.; Etourneau, J. Stabilization of a new superconducting phase by low temperature fluorination of La_2CuO_4. *Phys. C* **1990**, *167*, 97−101.

(3) de Laune, B. P.; Rees, G. J.; Whitaker, M. J.; Hah, H.-Y.; Johnson, C. E.; Johnson, J. A.; Brown, D. E.; Tucker, M. G.; Hansen, T. C.; Berry, F. J.; Hanna, J. V.; Greaves, C. Oxygen insertion reactions within the 1-D channels of phases related to $FeSb_2O_4$. *Inorg. Chem.* **2017**, *56*, 594−607.

(4) Fischer, R.; Pertlik, F. Refinement of crystal-structure of schafarzikite, $FeSb_2O_4$. *TMPM, Tschermaks Mineral. Petrogr. Mitt.* **1975**, *22*, 236−241.

(5) de Laune, B. P.; Greaves, C. Structural and Magnetic Characterisation of $CoSb_2O_4$, and the substitution of Pb^{2+} for Sb^{3+}. *J. Solid State Chem.* **2012**, *187*, 225−230.

(6) Giroux-Maraine, C.; Perez, G. Crystal-structure of magnesium antimonite, $MgSb_2O_4$. *Rev. Chim. Minerale* **1975**, *12*, 427−432.

(7) Cumby, J. C.; de Laune, B. P.; Greaves, C. The Structures and Magnetic Properties of $Fe_xCo_{1-x}Sb_2O_4$ and $Mn_xCo_{1-x}Sb_2O_4$, $0 \le x \le 1$. *J. Mater. Chem. C* **2016**, *4*, 201−208.

(8) Whitaker, M. J.; Bayliss, R. D.; Berry, F. J.; Greaves, C. The synthesis, structure, magnetic and electrical properties of $FeSb_{2-x}Pb_xO_4$. *J. Mater. Chem.* **2011**, *21*, 14523−14529.

(9) Fjellvåg, H.; Kjekshus, A.; Leskelä, T.; Leskelä, M.; Hoyer, E. Crystal and magnetic-structure of $MnSb_2O_4$. *Acta Chem. Scand.* **1985**, *39A*, 389−395.

(10) Witteveen, H. T. Magnetic susceptibility of $NiAs_2O_4$ and $NiSb_2O_4$. *Solid State Commun.* **1971**, *9*, 1313−1315.

(11) Gonzalo, J. A.; Cox, D. E.; Shirane, G. Magnetic structure of $FeSb_2O_4$. *Phys. Rev.* **1966**, *147*, 415−418.

(12) de Laune, B. P.; Whitaker, M. J.; Marco, J. F.; Thomas, M. F.; Berry, F. J.; Lees, M. R.; Greaves, C. Synthesis and magnetic characterisation of $Fe_{1-x}Mg_xSb_2O_4$ (x = 0.25, 0.50, 0.75) and their oxygen-excess derivatives, $Fe_{1-x}Mg_xSb_2O_{4+y}$. *J. Mater. Chem. C* **2017**, *5*, 4985−4995.

(13) de Laune, B. P.; Berry, F. J.; Marco, J. F.; Horswell, S. L.; Greaves, C. The Structure, Chemistry and Magnetic Properties of $FePbBiO_4$. *J. Mater. Chem. C* **2016**, *4*, 5320−5325.

(14) Rietveld, H. M. A profile refinement method for nuclear and magnetic structures. *J. Appl. Crystallogr.* **1969**, *2*, 65−71.

(15) Larson, C.; Von Dreele, R. B. General Structure Analysis System (GSAS). *Los Alamos National Laboratory Report LAUR* **2004**, 86−748.

(16) Toby, B. H. *J. Appl. Crystallogr.* **2001**, *34*, 210−213.

(17) Weenk, J. W.; Harwig, H. A. Calculation of electrostatic fields in ionic-crystals based upon Ewald method. *J. Phys. Chem. Solids* **1977**, *38*, 1047−1054.

(18) MacKenzie, K. J. D.; Smith, M. E. *Multinuclear Solid State NMR of Inorganic Materials*; Pergamon Press: Oxford, 2002.

(19) Harris, R. K.; Becker, E. D.; Cabral de Menezes, S. M.; Goodfellow, R.; Granger, P. NMR nomenclature: nuclear spin properties and conventions for chemical shifts. IUPAC Recommendations 2001. *Magn. Reson. Chem.* **2002**, *40*, 489−505.

(20) Massiot, D.; Fayon, F.; Capron, M.; King, I.; Le Calve, S.; Alonso, B.; Durand, J. O.; Bujoli, B.; Gan, Z. H.; Hoatson, G. Modelling one- and two-dimensional solid-state NMR spectra. *Magn. Reson. Chem.* **2002**, *40*, 70−76.

(21) Bayliss, R. D.; Berry, F. J.; de Laune, B. P.; Greaves, C.; Helgason, O.; Marco, J. F.; Thomas, M. F.; Vergara, L.; Whitaker, M. J. Magnetic interaction in ferrous antimonite, $FeSb_2O_4$, and some derivatives. *J. Phys.: Condens. Matter* **2012**, *24*, 276001.

(22) Gurusinghe, N. M. N.; Fones, J. C.; Marco, J. F.; Berry, F. J.; Greaves, C. Fluorine insertion into the Ruddlesden-Popper phase

DOI: 10.1021/acs.inorgchem.7b01613
Inorg. Chem. 2017, 56, 10078−10089

$La_2BaFe_2O_7$: the structure and magnetic properties of $La_2BaFe_2O_5F_4$. *Dalton Trans.* **2014**, *43*, 2038−2043.
(23) Belle, C.; Béguin, C.; Hamman, S.; Pierre, J.-L. F-19 NMR: An underused efficient probe for paramagnetic metal centers in bioinorganic solution chemistry. *Coord. Chem. Rev.* **2009**, *253*, 963−976.

DOI: 10.1021/acs.inorgchem.7b01613
Inorg. Chem. 2017, 56, 10078−10089